WORLD CONFERENCE ON TIMBER ENGINEERING 2025
BRISBANE, AUSTRALIA
Advancing Timber for the Future Built Environment

PREFABRICATED HOLLOW FLOOR SYSTEMS USING MASS PLY PANEL AND SCREW-GLUING

Tianci Huangfu[1], Maik Gehloff[2], Jianhui Zhou[3]

ABSTRACT: Floor construction can account for up to 70% of the wood used in mass timber buildings. Given that solid mass timber systems are not structurally efficient for long spans, there is increasing interest in composite floor systems. Structural composite lumber (SCL), which has a higher yield rate than lumber-based mass timber products, presents significant opportunities for mass timber construction. This study proposes a prefabricated hollow floor system based on SCL, utilizing a screw-gluing method. The efficacy of screw-glued joints in mass ply panel (MPP) was experimentally assessed, focusing on variations in screw spacing and screw types (partially and fully threaded self-tapping screws). Two types of polyurethane structural adhesives were also evaluated. Furthermore, a structural optimization algorithm was developed using Rhino/Grasshopper, employing a genetic algorithm for nonlinear optimization. Optimization targets included achieving optimal cross-sections while considering constraints such as load, span, geometry, and structural efficiency. Experimental results showed that the screw-glued joints can provide high shear connection capacity and stiffness with 100% wood failure, which can ensure almost full composite action for hollow floors. The optimization results demonstrated that MPP-based hollow floors significantly reduce material usage compared to traditional solid CLT and MPP systems, while maintaining or enhancing structural performance.

KEYWORDS: Mass ply panel, Screw-gluing, Hollow floor, Optimization

1 – INTRODUCTION

Floor construction can account for up to 70% of the wood material used in a mass timber building [1]. Solid mass timber floor systems, often constructed with lumber-based solid engineered wood products (EWP) such as cross-laminated timber (CLT) and glued laminated timber (glulam), can be structurally inefficient for long-span applications. This inefficiency stems from the inherent limitations of these materials: their bending stiffness values are relatively low, and the yield rate of lumber production is around 40-45%. Despite the environmental benefits of wood, optimizing material usage in floor systems is essential to reduce overall building material consumption. Structural composite lumber (SCL), such as laminated veneer lumber (LVL), mass plywood panel (MPP), laminated strand lumber (LSL), and parallel strand lumber (PSL), provides a higher yield rate of up to 90% and represents a viable alternative [2]. SCL products are produced as large-dimension billets with various strength grades and can be sawn into specified sizes, offering superior material utilization. Though SCL products have been produced in North America for over three decades, they have mainly been used in light wood framing.

Hollow floor systems are increasingly adopted by timber construction industries due to their high efficiency in material utilization and structural performance [3]. A ribbed CLT panel was developed, utilizing optimized dimensions to achieve the optimal structural design, and was fabricated by gluing with a hydraulic press [4]. In Europe, Metsä Group has developed a boxed/ribbed floor system based on LVL products with floor design software, which can provide optimal designs for varying requirements [5]. Stora Enso offers modular production of CLT-glulam composite rib floors and LVL-based hollow floors [6]. A common issue with these systems is that the production process often requires a large-dimension press for gluing. Recently, the screw-gluing method has been investigated for fabricating CLT-glulam composite floors for long-span applications [7-9]. The German standard [10] limits screw-gluing to 50 mm for flange thickness, while a study [11] showed that the axial clamping force provided by partially threaded self-tapping screws offers the necessary pressure for the adhesive between the CLT panel and glulam rib, even with larger thicknesses.

SCL billets can be manufactured and processed to any desired dimensions for flanges and webs. Therefore, combining SCL's flexibility with the material efficiency of hollow floors makes this floor system more adaptable and cost-effective. However, little research is available on the screw-gluing of SCL products. Moreover, current floor structural design practice relies on time-consuming manual iterative calculations, especially for hollow floors with various choices of member sizes and grades. Therefore, this study aims to develop a

[1] Tianci Huangfu, School of Engineering, University of Northern British Columbia, Prince George, Canada, huangfu@unbc.ca

[2] Maik Gehloff, School of Engineering, University of Northern British Columbia, Prince George, Canada, maik.gehloff@unbc.ca

[3] Jianhui Zhou, School of Engineering, University of Northern British Columbia, Prince George, Canada, jianhui.zhou@unbc.ca

https://doi.org/10.52202/080513-0190

prefabricated hollow floor system using SCL and screw-gluing, along with a parametric structural optimization tool.

2 – EXPERIMENTAL INVESTIGATION

2.1 MATERIALS

In this study, mass ply panel (MPP), a type of SCL produced by Freres Engineered Wood in Oregon, was used. The MPP used was F10 and F16 grade, manufactured from Douglas-fir veneers. The Young's modulus is 6205.3 MPa in the joist direction and 5860.5 MPa in the plank direction for the F10 grade, and 11032 MPa in the joist direction and 9653 MPa in the plank direction for the F16 grade [12-13].

According to DIN 1052-10:2012 [10], only partially threaded self-tapping screws (STS) should be used in the screw-gluing method. However, Aicher et al. [7] noted that fully threaded STS with varying pitch could also be used. Thus, HECO-TOPIX®-PLUS screws by HECO-Schrauben GmbH & Co. KG were employed in this study. The screws used included two types, partially threaded (P) and fully threaded (F). For the partially threaded type, lengths of 100 mm and 120 mm were used, while for the fully threaded type, lengths of 100 mm, 120 mm, and 160 mm were used. All screws had a diameter of 6 mm.

Two types of polyurethane structural adhesives were used for bonding between MPP ribs and flanges. LOCTITE HB X602 PURBOND (X602), a one-component polyurethane structural adhesive, served as the primary adhesive. It has an open time of 60 minutes and a minimum press time of 150 minutes at 20°C, with 65% relative humidity and a wood moisture content of 12%. However, the X602 adhesive is typically available in bulk quantities, which may be excessive for smaller projects. Therefore, an additional adhesive, LePage PL Premium Construction Adhesive Glue (PLMAX), was used for comparison. PLMAX has an open time of 20 minutes and a minimum press time of 24 to 48 hours at 25°C and 50% relative humidity.

2.2 SPECIMEN FABRICATION

Push-out test specimens were fabricated to assess the performance of the screw-gluing method compared to glue-only and screw-only groups, as well as to examine the effects of different adhesives and screw spacing. The specimens were assembled into I-shaped sections using 50mm thick MPP for both the flanges and webs, as illustrated in Figure 1. To facilitate the push-out tests, the rib and flange were offset by 50 mm to provide additional space. This adjustment made it easier to conduct the tests and handle the specimens during assembly and measurement. There were ten groups in total, including three screw-only groups, labelled as SF100, SF120 and SP100, with 100 mm and 120 mm long fully threaded and 100mm long partially threaded STS in 150 mm spacing, respectively. Two glue-only groups labelled as GF100 and GP100, with X602 adhesive. These two groups were assembled with fully threaded and partially threaded 100 mm long STS in 150 mm spacing, respectively, and then tested without the screws. Two groups with screw gluing method, labelled as 50_50_100F and 50_50_100P, consist of 100 mm long fully and partially threaded STS spaced in 150 mm and X602 adhesive, respectively. Two groups with screw gluing method, named 50_50_200s and 50_50_250s, were prepared with 100 mm long fully threaded STS and X602 adhesive, but in 200 mm and 250 mm spacing respectively. One last group called 50_50_PLMAX, with 100 mm long, fully threaded STS in 150 mm spacing, but used PLMAX as the adhesive. Four screws were used in each specimen, staggered 20 mm to each other in opposite direction, as shown in Figure 1. All the detailed group information is shown in Table 1.

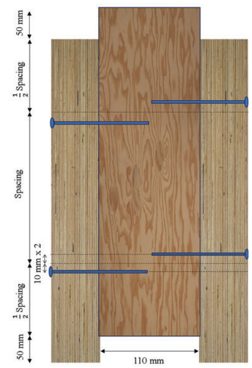

Figure 1. Schematic drawing of the test specimens

All screws were inserted at an angle of 90 degrees perpendicular to the flange, penetrating both the flange and the rib until the screw heads were flush with the outermost layer of the flange. All adhesives were applied according to the manufacturers' recommendations. For X602, an application rate of 160 g/m² was used as stated in manufacturer's product sheet. In contrast, the application rate for PLMAX was not explicitly quantified. Instead, it was described as applied using a 1/4-inch-wide nozzle. Therefore, in this experiment, PLMAX was applied in two parallel lines on the rib, as shown in Figure 2, to ensure the adhesive was evenly distributed across the surfaces of both the flange and the rib. The presence of slight adhesive squeeze-out along the bond line after pressure was applied indicated that enough adhesive had been applied, as shown in Figure 2. The amount of adhesive was measured as 1500 g/m².

Figure 2. Application of PLMAX

https://doi.org/10.52202/080513-0190

Table 1: Specimen information for push-out tests

Group	Replicates	Screw (mm)			Adhesive
		Length	Spacing	Type	
SF120	3	120	150	F	N/A
SF100	3	100	150	F	N/A
SP100	3	100	150	P	N/A
GF100	3	100	150	F	X602
GP100	3	100	150	P	X602
50_50_100P	6	100	150	P	X602
50_50_100F	6	100	150	F	X602
50_50_200s	3	100	200	F	X602
50_50_250s	3	100	250	F	X602
50_50_PLMAX	3	100	150	F	PLMAX

2.3 TESTING

Push-out shear tests were conducted in accordance with ASTM D5652-21 [14] with a rate of 2 mm/min. Two string potentiometers were installed on either side of each specimen, as shown in Figures 3, to measure the load-displacement curves.

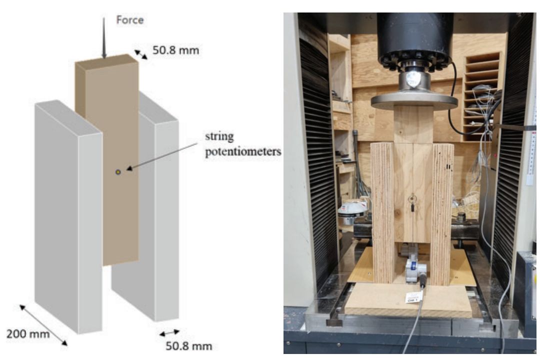

Figure 3. Push-out shear tests

After testing, the load-displacement curves for each specimen were plotted for analysis, and serviceability slip modulus (K_{ser}), ultimate slip modulus (K_u) and peak load were calculated. The surface failure percentage of the flange were estimated as well.

3 – PARAMETRIC DESIGN AND OPTIMIZATION

In this study, a structural optimization design tool for SCL prefabricated hollow-box floor module was developed in Rhinoceros 3D with its plugin Grasshopper for both closed (I-type) and open (T-type) hollow floors. This paper will focus on closed hollow floor as shown in Figure 4.

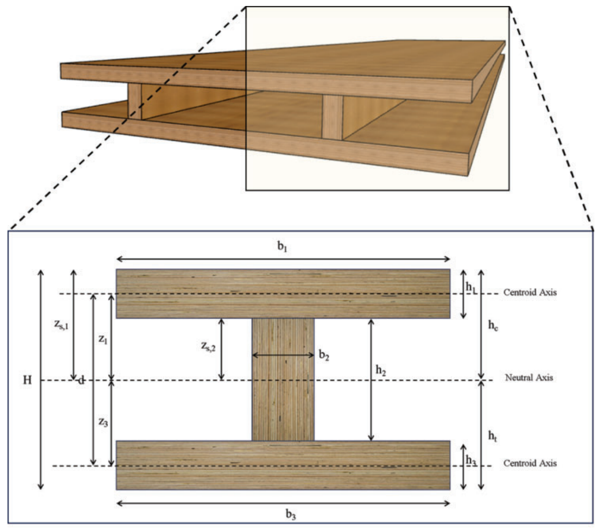

Figure 4. Concept of a SCL-based prefabricated floor module

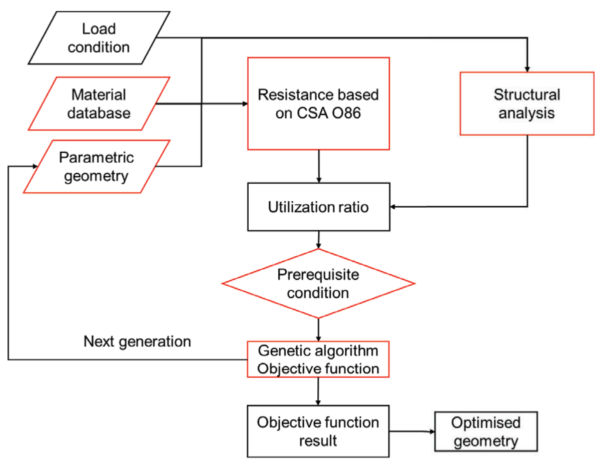

Figure 5. Flowchart of the parametric design and optimization tool

The optimization program consists of four main components: a parametric geometry model, a material database containing strength grades and design values, a CSA O86-based stressed skin panel design module, and an optimization module utilizing a genetic algorithm as shown in Figure 5. CSA O86 [15] provides design provisions for stressed skin panels. The standard introduces a calculation model based on the parallel-axis theorem, which assumes full composite action through gluing. The panel geometry reduction factor X_G, and the effective width can be calculated as follows,

$$X_G = 1 - 4.8\left(\frac{S_{clear}}{l}\right)^2 \tag{1}$$

$$b_{ef} = bX_G \tag{2}$$

where s_{clear} is the clear spacing between ribs, mm; l is the panel span, mm; b is the half of rib spacing, mm.

In this model, various parameters, such as the effective stiffness $(EI)_e$, bending moment resistance M_r, factored shear resistance of the rib at the neutral axis V_r, and factored shear resistance of the glued interface between the flange and rib V_{rp}, are calculated. Additionally, deflection Δ_s is determined using the equations provided in the standard, as detailed below:

$$(EI)_e = (EI)_w K_{SE} + b_f (b_{at} z_3{}^2 + b_{ac} z_1{}^2) K_s \tag{3}$$

where $(EI)_w$ is the stiffness of rib, Nmm^2; b_f is the total width of the panel, mm; b_{at} and b_{ac} are specified axial stiffness of tension and compression flange, respectively, N/mm.

To calculate bending moment resistance, the bending moment resistance in tension flange can be calculated as follows,

$$M_r = \emptyset_f T_p X_J X_G \frac{(EI)_e}{B_a K_S h_t} \tag{4}$$

$$T_p = t_p (K_D K_S K_T) \tag{5}$$

where $\emptyset_f$ is 0.95; t_p is specified strength capacity of flange in axial tension, N/mm; X_J is the stress-joint factor, can be found in CSA O86 Clause 10.4.

The bending moment resistance in compression flange can be calculated as follows,

$$M_r = \emptyset_f P_p X_J X_G \frac{(EI)_e}{B_a K_s h_c} \tag{6}$$

$$P_p = p_p (K_D K_S K_T) \tag{7}$$

where p_p is the specified strength capacity of flange in axial compression, N/mm.

Also, the calculation of bending moment resistance in the rib is shown below.

$$M_r = \emptyset_w F_b K_{zb} X_L X_G \frac{(EI)_e}{E K_{SE} c_w} \tag{8}$$

$$F_b = f_b (K_D K_{Sb} K_T K_H) \tag{9}$$

$$X_G = 1 - 4.8 (\frac{s_{clear}}{l})^2 \tag{10}$$

where $\emptyset_w$ is 0.9; f_b is the specified strength in bending of ribs, MPa; E is the Youngs's modulus of rib, MPa; s_{clear} is the clear spacing between longitudinal rib members, mm.

The following equations are used to calculate the shear resistance at the neutral plane,

$$V_r = \emptyset_w F_v K_{Zv} \frac{(EI)_e \sum b_g}{E K_{SE} \sum Q_w + B_a K_s b_{ef} max \begin{cases} z_1 \\ z_3 \end{cases}} \tag{11}$$

$$F_v = f_v (K_D K_{Sv} K_T K_H) \tag{12}$$

where f_v is the specified strength in shear of ribs, MPa; b_g is the contact width between flange and rib, mm; $\sum Q_w$ is sum of moments of area of all ribs about neutral plane, mm^3.

The flange-rib shear resistance for flange can be calculated as follows,

$$V_{rp} = \emptyset_f V_{gf} \frac{(EI)_e \sum (b_g X_{vf})}{B_a K_s b_{ef} max \begin{cases} z_1 \\ z_3 \end{cases}} \tag{13}$$

$$V_{gf} = v_{pf} (K_D K_S K_T) \tag{14}$$

where v_{pf} is the specified strength capacity in planar shear of the rib, MPa; X_{vf} is the shear-modification factor, see CSA O86 Figure 10.2.

To calculate the shear resistance to the rib, the following equations can be used.

$$V_{rp} = \emptyset_f V_{gw} \frac{(EI)_e \sum (b_g X_{vw})}{B_a K_s b_{ef} max \begin{cases} z_1 \\ z_3 \end{cases}} \tag{15}$$

$$V_{gf} = f_v (K_D K_S K_T) \tag{16}$$

where X_{vw} is 2.00, and the K factors are assumed as 1.

The deflection Δ_s can be calculated based on the formulas below:

$$\Delta_s = X_G \frac{5wl^4}{384(EI)_e} \tag{17}$$

The material database can include varies of material properties of SCL products, such as the elastic modulus, shear modulus, bending strength, shear strength, density and compression for both parallel and perpendicular to grain direction, etc. In this study, the F16 grade MPP from Freres Engineered Wood was used as the initial material for all the component of the panel in the database, while additional materials can be added to the material database in the future. The design values of F16 grade MPP are shown in Table 2.

Table 2: F16 grade MPP design values [12,13,16]

Properties	Joist direction	Plank direction
Bending strength (f_b) MPa	24.0	15.9
Young's modulus (E) MPa	11032	9653
Screw Shear modulus (G) MPa	527.8	461.9
Shear strength (f_v) MPa	3.3	0.97
Compression strength (f_{cp}) MPa	9.4	6.2
Tension strength (f_t)MPa	16.6	
Density at 12% MC (ρ) kg/m^3	550	

In accordance with the NBCC 2020 [17], two load scenarios were considered for this study: a live load of 1.9 kPa for bedrooms in residential areas and a live load of 2.4 kPa for office spaces. The worst-case load combination, $1.25D + 1.5L$, was applied for the ultimate limit state (ULS) design. The entire section was assumed as simply supported during

https://doi.org/10.52202/080513-0190

the calculation. For serviceability limit state design, the deflection limit Δ_r can be calculated according to the worst load combination, selected between $1.0D + 1.0L$ with a corresponding deflection limit of $L/180$ and $1.0L$ with a corresponding deflection limit of $L/360$.

The material properties and grades, as well as the thicknesses of the flange and rib, are defined as discrete variables. The thickness of component h_1 and b_2 can be cut from the MPP panels in increments of 25.4 mm, while the width of the flange b_2 and the height of the rib h_2 are considered continuous variables. For I sections, the upper and lower flange are always assumed to the same ($h_1 = h_3$).

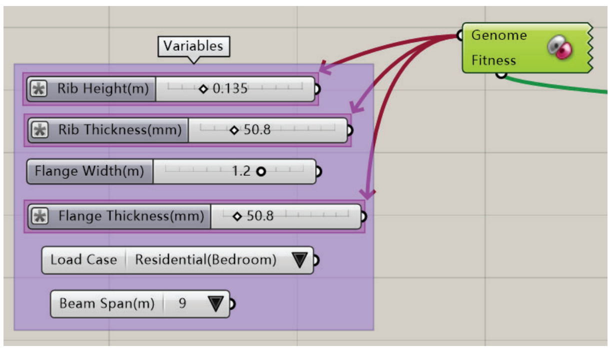

Figure 6. Input variables of optimization algorithm

The genetic algorithm component, Galapagos, was employed for the optimization of the cross-section design. During the optimization process, Galapagos adjusts the thickness of the flange, as well as the height and thickness of the rib, as illustrated in Figure 6. Comparing to I-joist and CLT panel, the ranges for these values are presented as flowing,

$$50\,mm \le h_2 \le \begin{cases} 800\,mm\ for\ l > 9000\,mm \\ 500\,mm\ for\ l \le 9000\,mm \end{cases} \tag{18}$$

$$25.4\,mm \le h_1 \le 254\,mm \tag{19}$$

$$25.4\,mm \le b_2 \le \begin{cases} 508\,mm\ for\ l > 9000\,mm \\ 254\,mm\ for\ l \le 9000\,mm \end{cases} \tag{20}$$

The total height of the section is constrained to a maximum of 500 mm for all spans, referencing the floor span table for wood I-joisted floors [17]. Additionally, the flange width b_1 can be manually selected within the range of 1200 mm to 2400 mm. Other parameters, such as the floor type, floor span, design live load, and all adjustment factors for wood design, need to be manually specified. The available span options for the optimization are 6 m, 9 m, or 12 m.

Then the algorithm will go through the CSA design method to obtain the bending moment and shear force resistance for current configuration, as well as the deflection. The design criteria for the genetic algorithm can be described as multiple equations. Equations 21-25 are used to calculate and prerequisite constraint of the algorithm, include utilization ratio of bending moment, shear force and deflection, the design check must be satisfied before entering objective function.

$$u_M = \frac{M_m}{M_r} < 1 \tag{21}$$

$$u_V = \frac{V_m}{min\begin{cases} V_r \\ V_{rp} \end{cases}} < 1 \tag{22}$$

$$u_d = \frac{\Delta_s}{\Delta_r} < 1 \tag{23}$$

where u_M is the ratio of the actual bending moment to the bending moment capacity. u_V is the ratio of the actual shear force to the shear force capacity. u_d is the ratio of the actual deflection to the deflection limit. Generally, deflection becomes the governing check for wood-based floor systems.

Additionally, the total height H can be constrained as well, by using the following,

$$H < 500\text{ mm} \tag{24}$$

Then the objective functions could be defined as following to consider the balance between floor height or volume,

$$objective\ function = a \times H + b\ \times V \tag{25}$$

where V is the total volume in m^3, and H is the floor height in mm, a and b are constant depending on user's optimization goal. a and b were set to be 0.01 and 100 in this study, respectively.

In this study, the setup for the genetic algorithm and the optimization process is illustrated in Figure 7. The initial geometry of the floor system is input into the genetic algorithm, which then iteratively modifies the design parameters to optimize structural performance. The algorithm evaluates each generation based on design criteria mentioned above. It selects the best-performing individuals to undergo mutation and crossover, ensuring that the next generation has improved design characteristics. This process continues until the optimal solution is found, balancing all the terms in the objective function. The term "Max stagnant" represents the number of generations the algorithm will run without improvement, while "population" refers to the number of individuals within each generation. "Initial boost" is a factor applied to the population size in the first generation to prevent the algorithm from prematurely converging to a local optimum. The "Maintain" term indicates the percentage of the best-performing individuals from each generation that are carried over to the next generation, while "inbreeding" refers to the breeding of solutions that share a very similar genetic makeup. In this case, the gene represents the variables controlled by Galapagos. Each generation consists of 30 individuals, evaluated based on the objective function. The population was set to 30, with an initial boost applied twice to gather sufficient samples. The top 30% of individuals were retained for the next crossover, while 70% shared similar genetic traits. Crossover continued until 40 generations were completed. After the optimization process was executed, optimized results for different spans and widths were obtained, which include minimum volume and minimum height results.

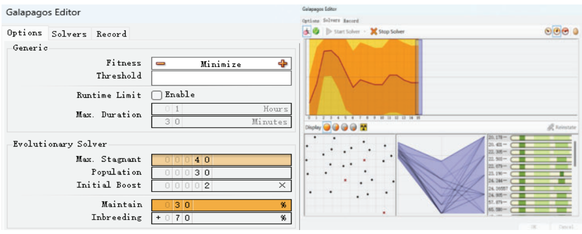

Figure 7. Galapagos settings and optimization process.

4 – RESULTS AND DISCUSSION

4.1 PUSH-OUT TEST RESULTS

Three screw-only groups were tested to compare the difference between partially threaded STS and fully threaded STS with the same screw length and diameter, as well as the effect of screw length. The typical load-displacement curves from each group are shown in Figure 8 and the failure modes are presented in Figure 9. In these three test groups, it can be observed that, compared to the other two groups, the SF120 group had higher initial connection stiffness. As observed in the failure modes shown in Figure 9, the screws yielded within the rib, leading to an embedment failure in the surrounding MPP.

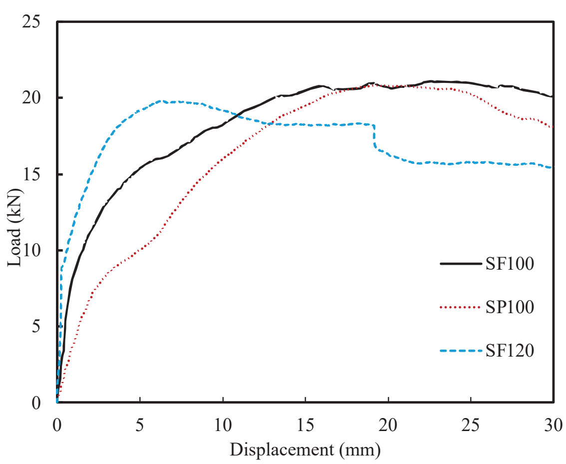

Figure 8. Typical load-displacement diagram of screw-only groups

Figure 9. Failure mode of screw-only group, glue-only group and screw-glue groups

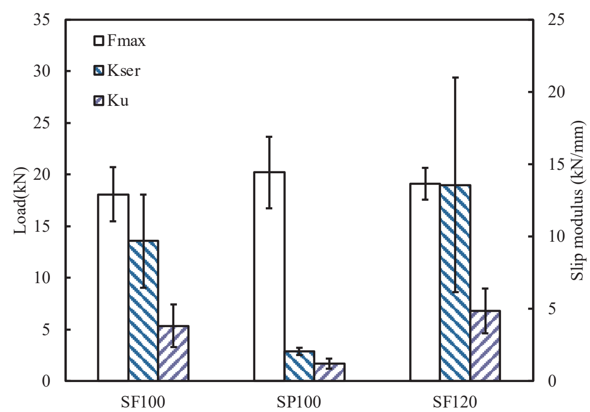

Figure 10. Load-carrying capacity and slip modulus of screw-only group

Figure 10 shows the load-carrying capacity, ultimate, and serviceability stiffness for each group with standard deviation error bars. All three groups had similar load-carrying capacity, ranging from 18 kN to 20 kN. The SF120 group had the highest K_{ser} of 19.0 kN/mm, followed by the 100F group at 13.6 kN/mm, while the 100P group had a significantly lower serviceability slip modulus of 2.9 kN/mm. The ultimate slip modulus values were 6.8 kN/mm, 5.37 kN/mm, and 1.7 kN/mm for SF120, SF100, and SP100, respectively.

Two glue-only connection groups were tested to evaluate the effectiveness of screw-gluing method. As shown in Figure 9 and 11, the failure mode showed that the veneer on the flange sheared off, causing the entire specimen to fail. Notably, the adhesive layer of X602 remained intact, with average surface failure percentages, calculated based on the proportion of the

https://doi.org/10.52202/080513-0190

damaged surface area to the total contact area through visual inspection, of 94% for GF100 and 83% for GP100. With 100 mm fully threaded STS, the F_{max} reaches to 79.8 kN, K_{ser} comes to 80.7 kN/mm, K_u is 94.5 kN/mm and shear stress τ_{avg} is 5.3 MPa. In contrast, for the GP100 group, F_{max} reaches to 67.8kN, K_{ser} comes to 94.2 kN/mm, K_u is 110.3 kN/mm and shear stress is 4.5 MPa. This demonstrates a higher load capacity in the GF100 group compared to the GP100 group, while the stiffness, or resistance to deformation, was greater in the GP100 group.

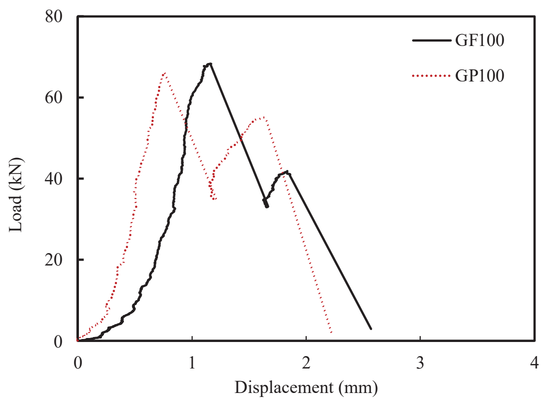

Figure 11. Typical load-displacement diagram of glue-only groups

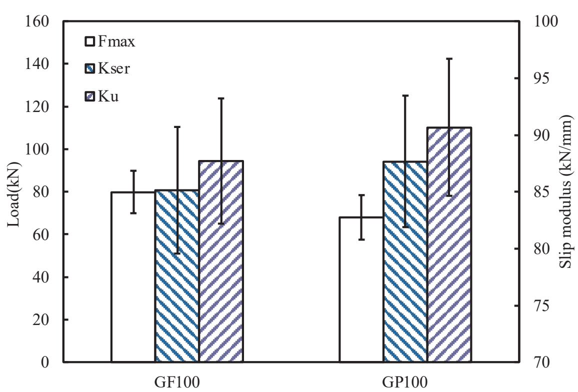

Figure 12. Load-carrying capacity and slip modulus of glue-only group

Three screw-glued groups were tested to compare the effects of different screw types and adhesives on connection performance. Figure 13 shows the typical load-displacement curves, and Figure 9 shows the failure modes. The load initially increased linearly with displacement, indicating elastic behaviour, until the load-carrying capacity was reached, followed by brittle failure in the veneer of the flanges. This failure mode was similar to that in the glue-only specimens. After reaching the load-carrying capacity, the load dropped sharply to 20-30% of the load-carrying capacity as displacement increased. The residual load was higher than in the screw-only groups, indicating better post-peak performance for screw-glued connections. The primary failure mode was veneer failure in the second layer of the flanges, with no failure in the glue lines at the flange or rib surface. This suggests that the screw-gluing method effectively maintained adhesive bond integrity under significant loading, with failure localized within the wood material.

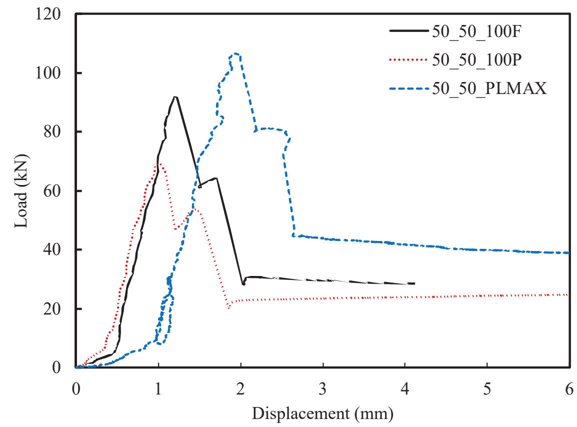

Figure 13. Typical load-displacement diagram of screw-glued groups

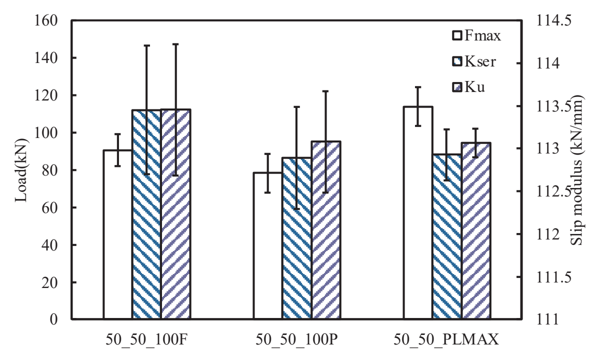

Figure 14. Load-carrying capacity and slip modulus of screw-glued group

According to Figure 14, when comparing the different screw and adhesive, the 50_50_PLMAX group shows the highest F_{max} of 113.9 kN, followed by the 50_50_100F group with 90.7 kN. The group with the lowest F_{max} is the 50_50_100P group with 78.4. K_{ser} are 88.2 kN/mm, 112.0 kN/mm and 86.5 kN/mm for 50_50_PLMAX, 50_50_100F and 50_50_100P groups, respectively. K_u are 94.6 kN/mm, 112.2 kN/mm and 95.1 kN/mm, respectively.

Four groups of screw-glued connections were compared to investigate the effects of different screw spacings on the connection performance. According to Figure 15, when all other conditions remained constant but screw spacing was increased, F_{max} increased from spacing 150 mm to 250 mm, but dropped from spacing 250 mm to 300 mm. For 150 mm spacing group, it has F_{max} of 90.7 kN, K_{ser} of 112.0 kN/mm and K_u of 112.2 kN/mm. For 200 mm spacing group, it has F_{max} of 92.3 kN, K_{ser} of 97.9 kN/mm and K_u of 99.7 kN/mm, for 250 mm spacing group, the F_{max} increased to 124.6 kN, but K_{ser} and K_u dropped to 83.3 kN/mm and 88.0 kN/mm, and for 300 mm spacing groups, the F_{max} is 120.3 kN, but K_{ser} and K_u increase to 136.7 kN/mm and 149.6 kN/mm respectively.

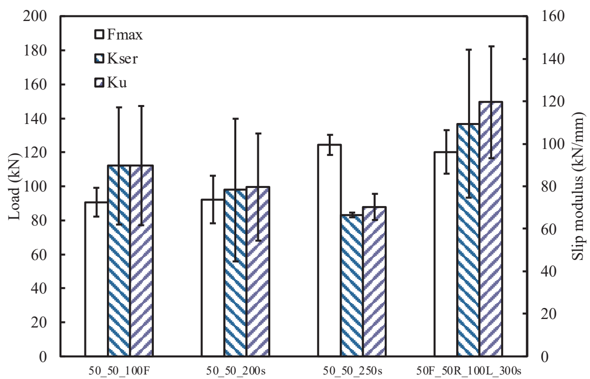

Figure 15. Load-carrying capacity and slip modulus of different spacing

4.2 OPTIMAL HOLLOW FLOOR DESIGN RESULTS

Based on the push-out tests, the screw-gluing method can provide high connection stiffness and strength, ensuring close to full composite action. Under the residential floor scenario (1.9 kPa), the optimization results based on ULS and deflection for both 1.2 m and 2.4 m widths and for each span (6 m, 9 m, 12 m) are shown in Table 3. The deflection utilization rate remained consistently high, ranging from 90% to 99%, which indicated that the designs were optimized close to the allowable deflection limits.

Table 3: Optimal MPP-based hollow floor modules

Properties	Floor span								
	6m			9m					12m
	Floor module width								
	1.2 m		2.4 m		1.2 m		2.4 m		2.4 m
h_2 (mm)	95	90	80	195	190	185	100	305	125
b_2 (mm)	50.8	228.6	50.8	50.8	101.6	50.8	101.6	50.8	101.6
h_1 (mm)	25.4	25.4	25.4	25.4	25.4	25.4	50.8	25.4	76.2
u_d (%)	96.1	98.2	94.5	95.8	90.0	97.2	99	97.1	94.3
u_M (%)	16.5	15.6	21.1	23.7	22.7	27.3	14.7	33.2	13.5
u_V (%)	26.4	7.7	61.0	20.3	9.4	44.9	36.5	37.2	40.2
H (mm)	145.8	140.8	130.8	245.8	240.8	235.8	201.6	355.8	277.4
V (m^3)	0.42	0.61	0.78	0.73	0.98	1.26	2.38	1.83	4.69

To compare the material usage of hollow-box floor module made from MPP with other materials, deflection and vibration should be considered in the serviceability limit state (SLS) design in condition of meeting ULS design. When considering deflection, the combination of dead load D was set to 2.0 kPa to facilitate comparison with other floor systems. According to [18] and [12], to achieve deflection-controlled span of 6 m with 2.0 kPa dead load, and 1.9 kPa live load, at least 5 ply CLT of 175 mm or 156 mm MPP solid floor must be used. For the I joist, according to Weyerhaeuser Company [19], at least 241 mm thick 230 TJI ® with 304 mm spacing and 18.3 mm-oriented strand board (OSB) sheathing should be used. For the 9 m span, at least 9 ply CLT or 207 mm thick MPP solid floor is required. For the I joist, at least 301 mm thick, 560 TJI ® with 304 mm spacing and 18.3 mm sheathing should be used. The detailed material usage for each type of floors with the same floor width 1.2 m is shown in Figure 16.

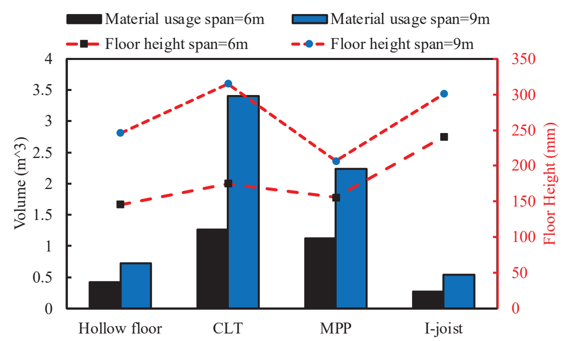

Figure 16 Material usage and floor height comparison for deflection-controlled criteria between 6m and 9m span and 1.2 m width

It can be seen that material usage for solid CLT is the highest in both span conditions, being approximately three times and four times that of the hollow-box floor module for 6 m and 9 m spans, respectively. Similarly, the MPP system requires substantially more material, with nearly 2.5 times the volume of the hollow-box floor module for the 6 m span and 3 times for the 9 m span. The I-joist system, on the other hand, uses around 50% and 70% of the material compared to the hollow-box floor module for the 6 m and 9 m spans, respectively. However, its floor height is about 60% and 20% greater than that of the hollow-box floor module for each span length. In contrast, both the CLT and MPP panels have higher material usage compared to the hollow-box floor module for both spans. While the floor height of these panels is similar to the hollow-box floor module in the 6 m span, the MPP system shows a reduced floor height in the 9 m span. The I-joist follows a consistent trend across both spans, using less material than the hollow-box floor module but requiring a greater floor height.

https://doi.org/10.52202/080513-0190

5 – CONCLUSION

This study has demonstrated that screw-gluing and parametric design can support the development of material and structural efficient SCL-based prefabricated hollow floor systems for long-span floor applications. The results can be summarized as follows:

1. Screw-gluing is a viable solution for creating effective bonding in MPP flange-to-rib connections, providing high stiffness and load-carrying capacity.
2. Screw-gluing connections achieved a remarkable stiffness of 112.18 kN/mm and a load-carrying capacity of 90.66 kN, far surpassing both screw-only and glue-only configurations.
3. Optimization results demonstrated that SCL-based hollow-box floor systems could achieve up to 70% material savings compared to CLT and MPP solid panel floor systems under ultimate limit state and deflection-controlled conditions.

Future research should investigate the structural performance of full-size floor modules through full-scale bending and vibration tests.

ACKNOWLEDGEMENTS

The project was funded by a BC FII Wood First Grant and Natural Sciences and Engineering Research Council of Canada Discovery Grant. The support from UNBC technicians James Andal and Nathan Downie is appreciated, and the in-kind materials donated by Freres Engineered Wood (MPP), Herrmann's – Quality Building Products (Heco screws), and Henkel (adhesives) are appreciated.

REFERENCES

[1] R. Brandner et al. "Cross laminated timber (CLT): overview and development." In: Eur. J. Wood Prod. 74 (2016) 331–351.

[2] Z. Gao, M. Gong. "Strand-Based Engineered Wood Products in Construction." In: Engineered Wood Products for Construction, IntechOpen, London, UK, 2021.

[3] A. Homb, S. Conta. "Timber hollow-box floors: Sound insulation measurement results and analysis." In: Build. Acoust. 29(3) (2022) 367–385.

[4] I. Sustersic, B. Dujic, S. Aicher. "Less is more—optimised ribbed CLT plates—the future." In: N.Z. Timber Des. J. 25(2) (2017) 19–26.

[5] Metsä Group. "Benefits of building with Kerto LVL - Webinar recording." https://www.metsagroup.com/metsawood/news-and-publications/videos/benefits-of-building-with-kerto-lvl-tomorrow/, last accessed 2024/03/09.

[6] Stora Enso. "Rib panels." https://www.storaenso.com/en/products/mass-timber-construction/building-products/rib-panels, last accessed 2024/03/09.

[7] S. Aicher, N. Zisi, K. Simon. "Screw-gluing of ribbed timber elements—effects of screw spacing and plate stiffness on bond line cramping pressure." In: Otto Graf J. 20 (2021) 9–38.

[8] K. Bratulic, M. Augustin. "Screw gluing—theoretical and experimental approach on screw pressure distribution and glue line strength." In: Proc. WCTE, Vienna, Austria, 2016.

[9] M. Shahnewaz, C. Dickof, J. Zhou, T. Tannert. "Vibration and flexural performance of cross-laminated timber–glulam composite floors." In: Compos. Struct. 292 (2022) 115682.

[10] DIN 1052-10:2012. Design of Timber Structures - Part 10: Additional Provisions. German Institute for Standardization (DIN), Berlin, Germany, 2012.

[11] M. Kairi. "Screw gluing gives new possibilities for wood engineering." In: Proc. Int. Timber Constr. Conf., Biel, Switzerland, 2000, pp. 5.

[12] Freres Engineered Wood. https://frereswood.com/products-and-services/mass-ply-products/mass-ply-panel/, last accessed 2024/03/15.

[13] R. Soti, T.X. Ho, A. Sinha. "Structural performance characterization of mass plywood panels." In: J. Mater. Civ. Eng. 33(10) (2021) 04021275.

[14] ASTM International. ASTM D5652-21: Standard Test Methods for Single-Bolt Connections in Wood and Wood-Based Products. ASTM International, West Conshohocken, PA, 2019.

[15] Canadian Standards Association (CSA). O86-24: Engineering Design in Wood Standard. CSA Group, Mississauga, ON, 2024.

[16] T. Ho, A. Arora, A. Sinha. "In-plane shear properties of mass ply panels in long-ply direction." In: J. Mater. Civ. Eng. 34(8) (2022) 241–252.

[17] National Research Council of Canada (NRCC). National Building Code of Canada 2020. Canadian Commission on Building and Fire Codes, Ottawa, ON, 2020.

[18] Canadian Wood Council. Wood Design Manual 2017. Canadian Wood Council, Ottawa, ON, 2017.

[19] Weyerhaeuser Company. TJI® 110, TJI® 210, TJI® 230, TJI® 360, TJI® 560, and TJI® 560D Joists Featuring Trus Joist® TJI® Joists for Floor and Roof Applications. https://www.weyerhaeuser.com/woodproducts/document-library/, last accessed 2024/03/15.